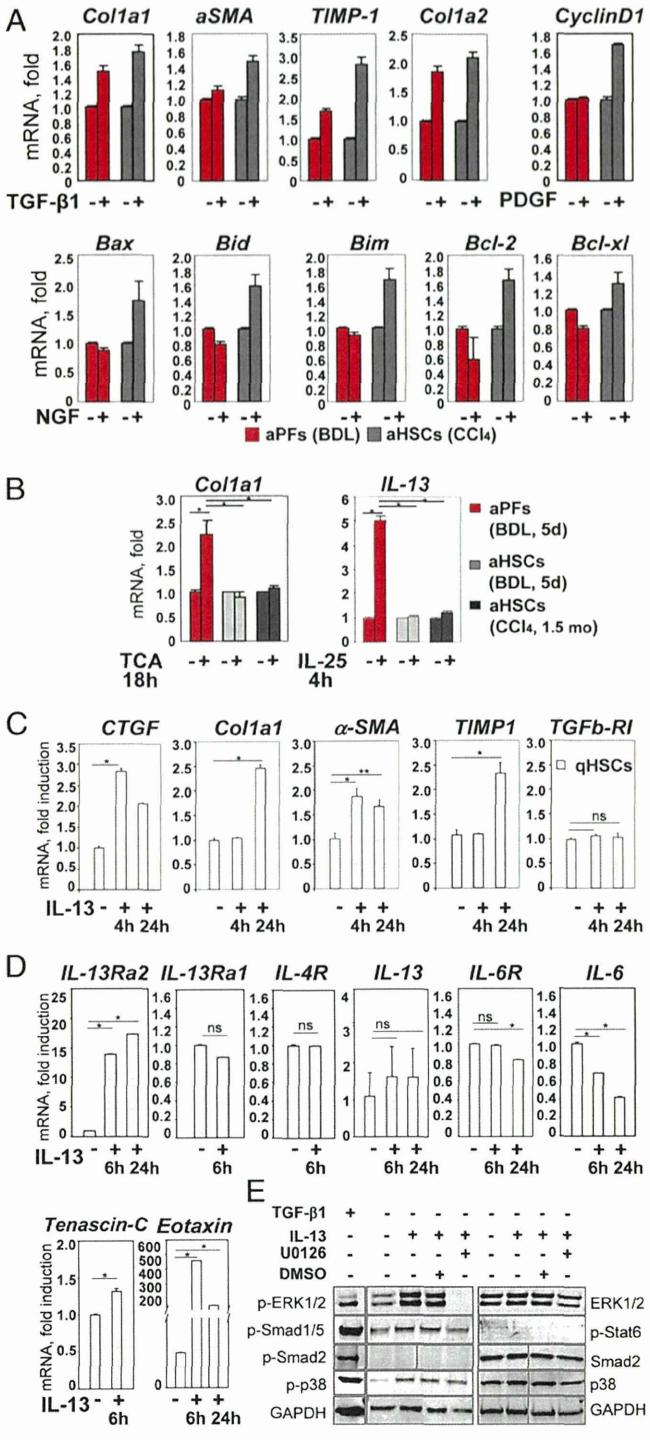

Fig. 4. Functional properties of aPFs and aHSCs. (*A*) Response to cytokines was compared in BDL-aPFs and CCl_4-aHSCs. Both aHSCs and aPFs responded to TGF-β1 (10 ng/mL). aHSCs, but not aPFs, responded to PDGF (100 pg/mL) and NGF (100 ng/mL). The data are fold induction compared with untreated aPFs (or aHSCs), $P < 0.01$. (*B*) BDL-aPFs (but not BDL-aHSCs or CCl_4-aHSCs) responded to bile acid taurocholic acid (TCA; 1,200 nmol/mL) by up-regulation of *Col1a1*, and to IL-25 (100 ng/mL) by IL-13 secretion, $P < 0.05$. Stimulation of aPFs with Tauro-ursodeoxycholate (TUDCA; 25 nmol/mL), deoxycholic acid (DCA; 0.1 nmol/mL), taurochenodeoxycholate (TCDCA; 60 nmol/mL), Tauro b-muricholate (TbMCA; 2,000 nmol/mL), and cholic acid (CA; 20 nmol/mL) did not result in Col1a1 induction. The data are fold induction compared with untreated aPFs (or aHSCs), $*P < 0.05$. (*C*) The effect of IL-13 on HSC activation was evaluated. qHSCs were incubated with IL-13 (100 ng/mL) for 4 h and 24 h. Gene expression was evaluated by RT-PCR, $*P < 0.01$; $**P < 0.02$; ns, nonsignificant. The data (*A–C*) represent three independent experiments. For each experiment, the cells were isolated from three mice. (*D*) IL-13 signaling in mouse HSCs: IL-13–stimulated HSCs (100 ng/mL, 6 h) up-regulate IL-13Rα2, tenascin C, and eotaxin, but do not express IL-13 or IL-6, as shown by RT-PCR. (*E*) IL-13 signaling in HSCs (2 h) causes phosphorylation of ERK1/2 (which is blocked by ERK inhibitor U0126, 10 μM), p38, and Smad1/5, as shown by Western blot. TGF-β1–stimulated HSCs served as a control.

aHSCs and aPFs Are the Major Source of Myofibroblasts in Fibrotic Liver. Although vitamin A-rich lipid droplets are a distinctive characteristic of HSCs, activation results in a decrease in these droplets (1). However, in vivo aHSCs do not lose their vitamin A droplets completely, and vitamin A-induced buoyancy has become a standard way to purify quiescent and aHSCs in vivo, as confirmed by gene expression profiling (25, 41). Our current study provides additional proof that vitamin A is a reliable marker for identification, quantification, and purification of aHSCs, making flow cytometry using vitamin A autofluorescence as the method of choice to purify aHSCs from myofibroblasts of other origins. Flow cytometry enables identification of hepatic myofibroblasts and isolation of distinct subsets of myofibroblasts (HSCs and PFs) with high purity from the same mouse liver.

Using collagen-GFP reporter mice, we demonstrate that the total population of GFP^+ myofibroblasts isolated in the nonparenchymal fraction consists of two major populations: $Vit.A^+$ aHSCs and $Vit.A^-$ aPFs. These results were confirmed by immunostaining for cell-specific markers, RT-PCR, and gene expression microarrays. Specifically, aHSCs were identified as $Vit.A^+$, $GFAP^+$, $Desmin^+$, and $CD146^+$ cells that exhibit specific morphology. In turn, $Vit.A^-$ aPFs lacked GFAP or Desmin expression, but were characterized by expression of Thy1 and Elastin, and a more round-shaped morphology. Collectively, HSCs and PFs contribute to more than 94% of GFP^+ myofibroblasts. This type of analysis should now be extended to other experimental models of liver fibrosis, such as alcohol-induced liver disease and nonalcoholic steatohepatitis.

aHSCs and aPFs Contribute Differently to Liver Fibrosis of Different Etiologies. Although the role of aPFs in the development of portal fibrosis has been discussed (42, 61), our study is the first to our knowledge to quantify the myofibroblast populations over a time course. Consistent with previous studies (62, 63), we demonstrate that aPFs play an important role at early stages of BDL-induced liver fibrosis (13) by contributing >70% of myofibroblasts. Moreover, even at later stages (BDL, 17–20 d), aPFs contribute ~50% of myofibroblasts and exhibit a more activated phenotype than aHSCs. Thus, the composition of myofibroblasts varies depending on the etiology and time course of liver injury and fibrosis.

Cholestatic Injury Induces Predominant Activation of aPFs. The mechanism of fibrogenesis differs in CCl_4 and BDL models of liver injury. Treatment with CCl_4 is hepatotoxic, causing necrosis of hepatocytes and inflammation in the pericentrolobular area. However, BDL induces obstruction of bile flow with increased biliary pressure, moderate inflammation, and cytokine secretion by biliary epithelial cells (64). Diffusion (accumulation) of free bile acids may trigger ductular reaction (hyperplastic response of bile duct epithelial cells), resulting in activation of cholangiocytes and portal fibroblasts. The mechanism of PF activation is poorly understood. Here, we propose that TCA bile acid can directly activate PFs (but not HSCs) into myofibroblasts, and this effect may rely on TCA-induced induced cytotoxicity, because PFs have been reported to lack the bile acid receptors FXR (farnesoid X receptor) and TGR5 (the membrane G protein-coupled

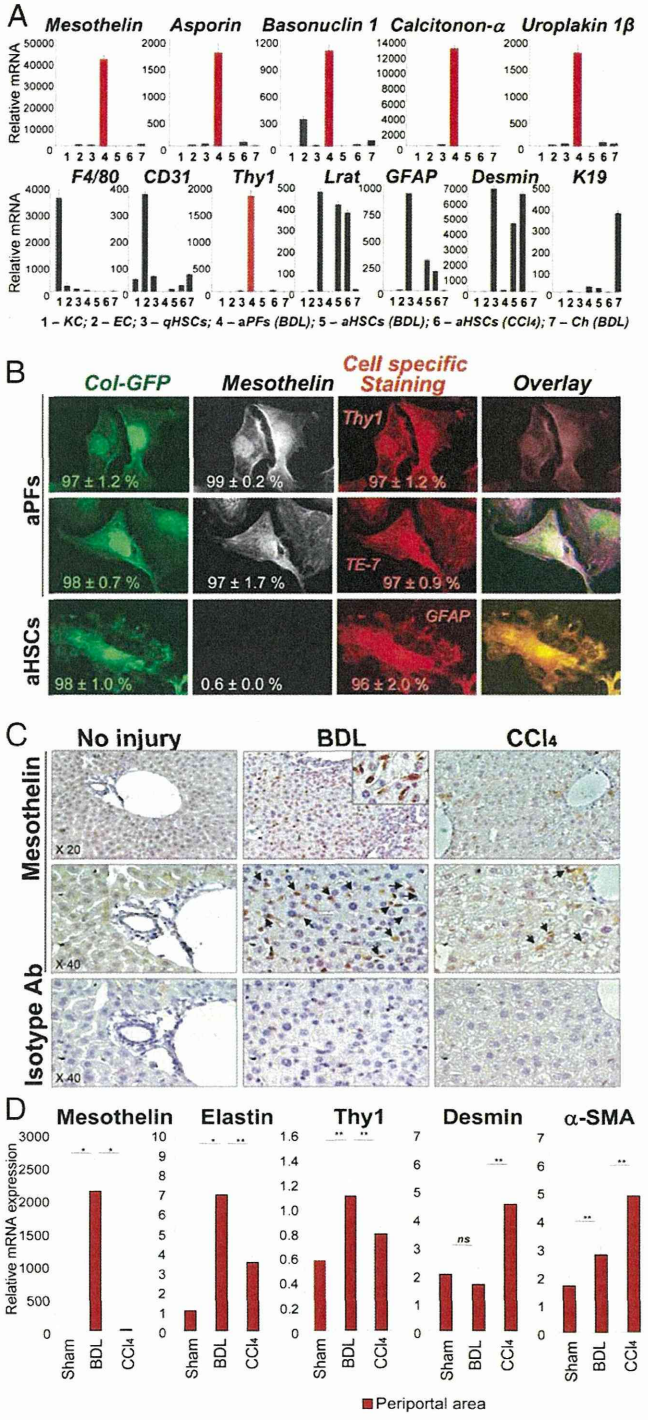

Fig. 5. Expression of mesothelin in aPFs is associated with cholestatic liver fibrosis in mice. (*A*) Expression of selected signature genes was compared by RT-PCR in aPFs and other cells in the liver. *Mesothelin, asporin, basonuclin 1, calcitonin-α,* and *uroplakin 1β* mRNA were up-regulated in BDL- (17 d) aPFs, but not in KC, endothelial cells (EC), BDL- and CCl_4-aHSCs and qHSCs, or BDL-induced cholangiocytes (Ch). The purity of each fraction was estimated by expression of F4/80 in KC, CD31 in EC, Lrat, GFAP, and Desmin in HSCs, Thy1 in aPFs, and K19 in cholangiocytes. The data (from three independent experiments) are shown as relative mRNA expression, $P < 0.01$. (*B*) aPFs and aHSCs were isolated from BDL (17 d)-injured Col-GFP mice and stained with anti-mesothelin Ab. Expression of Mesothelin was detected only in aPFs (but not in $GFAP^+$ aHSCs) and colocalized with Elastin (TE-7) and Thy1 staining. The percent of immunostained cells is calculated, $P < 0.05$ (four independent experiments; Fig. S7*B*). (*C*) Paraffin sections of liver tissue from BDL- (17 d) or CCl_4- (1.5 mo)treated mice ($n = 4$ per group) were immunostained with anti-mesothelin antibody or isotype-matched control. Expression of mesothelin was detected in BDL mice but not in sham-operated mice. Only a few mesothelin positive cells were detected in CCl_4-treated mice. Representative images are shown using 20× and 40× objective, (Fig. S7*C*). (*D*) Up-regulation of mesothelin is detected by laser capture microdissection in BDL-induced (but not CCl_4-induced) liver fibrosis. Laser capture microdissection was used to isolate periportal myofibroblasts from BDL (20 d) mice and CCl_4 (1.5 mo)-treated mice ($n = 3$ per group), cells were analyzed by RT-PCR for expression of aPF- and aHSC-specific markers. Mesothelin, elastin, and Thy1 were highly expressed in myofibroblasts obtained from periportal area of BDL liver. Desmin was expressed at high levels in CCl_4-treated liver. Unlike desmin, mesothelin was not expressed in CCl_4-treated periportal area. The data (from three independent experiments) are mRNA fold induction compared with periportal area of sham mice, $*P < 0.01$; $**P < 0.05$; ns, non-significant.

receptor) (65, 66). TCA-induced activation of PFs appears to be specific, and stimulation with other bile acids (TUDCA, DCA, TCDCA, TbMCA, CA) did not induce fibrogenic gene expression in PFs. However, unresponsiveness of PFs to tested bile acids may result from already high activation of isolated PFs (5 d after BDL), the lack of corresponding receptors (65), or poor experimental conditions (67). In addition, individual bile acids may produce other effects on PFs, such as cellular proliferation and cytokine secretion (17), which were not evaluated in this study. Furthermore, our in vitro conditions may not mimic the complex liver microenvironment required for bile acid stimulation of PFs (17). Alternatively, bile acids may indirectly induce PF activation by affecting cholangiocytes (68) or hepatocytes (65) that, in turn, may facilitate selective aPF activation via cell-cell signaling or cytokine secretion (64). In addition, specific factors produced by activated cholangiocytes may presensitize PFs for bile acid stimulation (69).

aPFS May Facilitate Activation of HSCs in BDL Model of Liver Injury. Another characteristic feature of aPFs is expression of IL-25R. Up-regulation of proinflammatory IL-17A, IL-25, IL-22, and IL-6 in the serum and in the liver accompany development of BDL-induced liver fibrosis (28). Therefore, it is not surprising that IL-25 may stimulate aPFs. Similar to other cell types, IL-25 induced secretion of IL-13 by aPFs, but did not further their activation. IL-13 has been implicated in pathogenesis of *Schistosoma mansoni* infection-induced liver fibrosis (70), and recently IL-13 was shown to directly stimulate HSCs to produce CTGF and subsequently upegulate fibrogenic genes in response to nonparasite liver injury (71). Therefore, we hypothesized that following BDL, IL-25–stimulated aPFs secrete IL-13, which facilitates HSC activation (via induction of *IL-13Ra2*, *Col1a1*, *Eotaxin*, *Tenascin-C*, *fibronection*, and phosphorylation of ERK1/2). Supporting this notion, bone marrow transplantation in $Abcb4^{-/-}$ mice lessened hepatic fibrosis via Th1 responses, but did not alter the level of IL-13 production (72), suggesting there must be an endogenous source of IL-13 in these mice. Further studies are required to determine the mechanism of HSC activation in response to cholestatic liver injury.

Proposed Novel Markers of Portal Fibroblasts. Robust markers of aHSCs and aPFs are needed. Our data confirmed that expression of Thy1 and Elastin distinguishes $Vit.A^-GFAP^-Desmin^-CD146^-$ aPFs from $Vit.A^+GFAP^+Desmin^+CD146^+Thy1^-Elastin^-$ aHSCs. Using gene expression profiling of in vivo aHSCs and aPFs, we have identified that mesothelin, calcitonin α, uroplakin 1β, basonclin 1, asporin, IL-18R1, and IL-25R may serve as additional useful markers to distinguish aPFs from aHSCs and myofibroblasts of other origins. We determined that these genes are highly expressed in portal fibroblasts but not in other cell types in fibrotic liver.

Interestingly, aPFs express mesothelin, calcitonin α, uroplakin 1β, basonclin 1, asporin, and IL-18R1 genes. The hepatic mesothelium is the source of HSCs and PFs during development (51, 60). Previous studies have demonstrated that the genes mentioned above and other genes [e.g., glycoprotein m6a, mesothelin, Uroplakin 1β and 3 β, Cyp2s1, mucin 16, crystalline, Prss12, Slipi, Caveolin, Dermokin, Calcitonin-related peptide, vanin, cytokeratin 7, Slc9a3r1, and Slc39a8 (metal ion transporter)], Igfbp6, see Fig. S6) are expressed in hepatic mesothelium (48). Furthermore, the gene expression profiles of epicardium isolated from adult mouse infarction-injured hearts identified the same genes among epicardium-specific signature genes, and for the first time, to our knowledge, implicated these genes (alone or in combination) in wound healing (49). Morphological studies have suggested that septum transversum mesenchyme (STM) is the source of hepatic mesenchymal cells (HSCs and perivascular mesenchymal cells) (73) and cardiac mesoderm [that gives rise to epicardium (74)]. Therefore, a common origin of hepatic mesothelium and epicardium may explain the similarity of gene expression profile of these tissues. During development, hepatic mesothelium undergoes an epithelial-to-mesenchymal (EMT) transition to produce PFs and HSCs. Furthermore, the expression of WT1, a mesothelial-specific factor (60), is expressed in aPFs (vs. aHSCs; Fig. S6). Because both hepatic mesothelium and epicardium can contribute to myofibroblasts in their respective organs, the contribution of the aforementioned genes to repair and fibrosis should be addressed.

Mesothelin is a glycosyl phosphatidylinositol (GPI)-anchored membrane glycoprotein that is expressed in normal mesothelial cells. It is also highly expressed in several species of malignant tumors, such as mesothelioma as well as ovarian and pancreatic cancers (75–77). We determined that mesothelin (Msln)-deficient mice are less susceptible to liver fibrosis compared with the wild-type mice. Previous studies have implicated mesothelin in mediation of cellular interaction and metastatic dissemination. Because of a strong induction in different types of cancer, mesothelin is considered as a tumor-associated antigen, which serves as a prognostic marker of disease progression, and became a therapeutic target for anti-cancer therapy. Here we demonstrate that mesothelin is highly expressed in aPFs in response to BDL, so that mesothelin may serve as a novel marker of aPFs and a potential target for antifibrotic therapy.

Materials and Methods

Mice and Liver Injury. Collagen α1(I)-GFP mice (22) and wild-type littermates were used at 8 wk of age, in C57BL/6 background. Liver injury was induced in mice by CCl_4 (1:4 dilution in corn oil, 60 μL × 14 injections; ref. 41) or ligation of the common bile duct (20 d) (41). Mice were maintained under specific pathogen free conditions at the animal facilities of University of California, San Diego (protocol S07088 approved by Institutional Animal Care and Use Committee).

Isolation of Nonparenchymal Fraction. Livers were perfused and digested by using the pronase/collagenase method (41), and cells were centrifuged to pellet the hepatocytes. The remaining nonparenchymal cell fraction [containing hepatic myofibroblasts (HSCs, portal fibroblasts, and others), Kupffer cells, BM cells, and endothelial cells] (41). aPFs and aHSCs were isolated by using cell sorting for Col-GFP$^+$Vit.A$^-$ and Col-GFP$^+$Viat.A$^+$ cells. Kupffer cells (KC) and endothelial cells were isolated by gradient centrifugation (15% Nycodenz) following by magnetic sorting with anti-CD11b and anti-CD31 antibodies, respectively (Miltenyi Biotec). Cholangiocytes were a gift of Gianfranco Alpini (Texas A&M Health Science Center, Central Texas Veterans Health Care System, Temple, TX) and were isolated from BDL mice (78).

Flow cytometry. Flow cytometry was based on simultaneous detection of collagen-α1(I)-GFP (488 nm) and vitamin A (autofluorescent signal detected by violet laser at 405 nm; Fig. 2*B*) in Col-GFP mice (40). Phenotyping of the nonparenchymal fraction isolated from Col-GFP mouse livers (n = 6 time point) was performed on Canto (BD). Cell sorting was performed on a MoFlo (Beckman Coulter).

Immunofluorescence and immunohistochemistry. Formalin-fixed frozen livers were stained with Sirius Red and anti–α-SMA Ab (Abcam). Immunohistochemistry was performed by using DAB staining (Vector) and counterstaining with Hematoxilin. Immunocytochemistry is described in *SI Materials and Methods*.

Whole Mouse Genome Gene Expression Microarray. The gene expression profile of qHSCs, CCl_4- (1.5 mo) aHSCs, BDL- (20 d) aHSCs, and PFs was studied by using Whole Mouse Genome Microarray (Agilent) (40). See *SI Materials and Methods* for details.

Characterization of IL-13 Signaling in Human HSCs. Human stellate cells (ScienCell) were plated overnight, then serum-starved for 6 h and stimulated with IL-13, TGFβ1 (R&D Systems), or a combination of both. CCL11/eotaxin was measured in cell-free supernatants 48 h after stimulation with IL-13 by sandwich ELISA (RnD Systems). Gene expression was assessed at 24 h by quantitative RT-PCR.

Quantitative RT-PCR. Total RNA was isolated from the nonparenchymal fraction, hepatocyte fraction, or purified Col$^+$Vit.A$^+$ and Col$^+$Vit.A$^+$ cells or hepatic stellate cells by using RNeasy columns (Qiagen). Gene expression levels were calculated after normalization to the standard housekeeping gene 18S by using the ΔΔ CT method as described by the manufacturer (Invitrogen) and expressed as relative mRNA levels compared with control. The results are represented as mean ± SEM, $P < 0.0001$.

Laser Capture Microdissection and RNA Extraction. Livers from sham-, CCl_4- and BDL-injured mice were snap-frozen in FSC 22 Frozen Section Media (Leica Microsystems) and stored at −80 °C. Transverse sections (10 μm) were cut with a cryostat at −20 °C. Cryosections were mounted on membrane-coated slides. A Leica LMD7000 system (Leica Microsystems) was used to cut periportal or centrilobular area on sections. Microdissected sections were collected in the lid of a 0.5-mL microtube containing RLT buffer from the RNeasy (Qiagen). Total RNA was extracted by using the same kit and following the manufacturer's instructions.

ACKNOWLEDGMENTS. We thank Dr. Sato and Dr. Uehiro for initial technical assistance with laser capture microdissection and Tom Kisby and Rebecca Dunmore for technical assistance with the in vitro studies using human HSCs. This work was supported by National Institutes of Health Grants DK088837, GM41804, AA15055, DK72237, AI0777802, and P50 AA011999; the Japanese Ministry of Health, Labour, and Welfare; and the American Liver Foundation.

1. Bataller R, Brenner DA (2005) Liver fibrosis. *J Clin Invest* 115(2):209–218.
2. Forbes SJ, Parola M (2011) Liver fibrogenic cells. *Best Pract Res Clin Gastroenterol* 25(2):207–217.
3. Kisseleva T, et al. (2006) Bone marrow-derived fibrocytes participate in pathogenesis of liver fibrosis. *J Hepatol* 45(3):429–438.
4. Kisseleva T, et al. (2011) Fibrocyte-like cells recruited to the spleen support innate and adaptive immune responses to acute injury or infection. *J Mol Med (Berl)* 89(10):997–1013.
5. Scholten D, et al. (2011) Migration of fibrocytes in fibrogenic liver injury. *Am J Pathol* 179(1):189–198.
6. Kalluri R (2009) EMT: When epithelial cells decide to become mesenchymal-like cells. *J Clin Invest* 119(6):1417–1419.
7. Choi SS, Diehl AM (2009) Epithelial-to-mesenchymal transitions in the liver. *Hepatology* 50(6):2007–2013.
8. Taura K, et al. (2010) Hepatocytes do not undergo epithelial-mesenchymal transition in liver fibrosis in mice. *Hepatology* 51(3):1027–1036.
9. Scholten D, et al. (2010) Genetic labeling does not detect epithelial-to-mesenchymal transition of cholangiocytes in liver fibrosis in mice. *Gastroenterology* 139(3):987–998.
10. Chu AS, et al. (2011) Lineage tracing demonstrates no evidence of cholangiocyte epithelial-to-mesenchymal transition in murine models of hepatic fibrosis. *Hepatology* 53(5):1685–1695.
11. Dranoff JA, Wells RG (2010) Portal fibroblasts: Underappreciated mediators of biliary fibrosis. *Hepatology* 51(4):1438–1444.
12. Bhunchet E, Wake K (1992) Role of mesenchymal cell populations in porcine serum-induced rat liver fibrosis. *Hepatology* 16(6):1452–1473.
13. Desmoulière A, et al. (1997) Extracellular matrix deposition, lysyl oxidase expression, and myofibroblastic differentiation during the initial stages of cholestatic fibrosis in the rat. *Lab Invest* 76(6):765–778.
14. Uchio K, et al. (2002) Cellular retinol-binding protein-1 expression and modulation during in vivo and in vitro myofibroblastic differentiation of rat hepatic stellate cells and portal fibroblasts. *Lab Invest* 82(5):619–628.
15. Wen JW, Olsen AL, Perepelyuk M, Wells RG (2012) Isolation of rat portal fibroblasts by in situ liver perfusion. *J Vis Exp* (64):3669.
16. Kruglov EA, Jain D, Dranoff JA (2002) Isolation of primary rat liver fibroblasts. *J Investig Med* 50(3):179–184.

17. Clouzeau-Girard H, et al. (2006) Effects of bile acids on biliary epithelial cell proliferation and portal fibroblast activation using rat liver slices. *Lab Invest* 86(3): 275–285.
18. Knittel T, et al. (1999) Rat liver myofibroblasts and hepatic stellate cells: Different cell populations of the fibroblast lineage with fibrogenic potential. *Gastroenterology* 117(5):1205–1221.
19. Goodpaster T, et al. (2008) An immunohistochemical method for identifying fibroblasts in formalin-fixed, paraffin-embedded tissue. *J Histochem Cytochem* 56(4): 347–358.
20. Dranoff JA, et al. (2002) The ecto-nucleoside triphosphate diphosphohydrolase NTPDase2/CD39L1 is expressed in a novel functional compartment within the liver. *Hepatology* 36(5):1135–1144.
21. Bosselut N, et al. (2010) Distinct proteomic features of two fibrogenic liver cell populations: Hepatic stellate cells and portal myofibroblasts. *Proteomics* 10(5):1017–1028.
22. Yata Y, et al. (2003) DNase I-hypersensitive sites enhance alpha1(I) collagen gene expression in hepatic stellate cells. *Hepatology* 37(2):267–276.
23. Brenner DA, Rippe RA, Veloz L (1989) Analysis of the collagen alpha 1(I) promoter. *Nucleic Acids Res* 17(15):6055–6064.
24. Österreicher CH, et al. (2010) Fibroblast specific protein 1 identifies a subpopulation of liver inflammatory macrophages. *Proc Natl Acad Sci USA* 108(1):308–13.
25. De Minicis S, et al. (2007) Gene expression profiles during hepatic stellate cell activation in culture and in vivo. *Gastroenterology* 132(5):1937–1946.
26. Inokuchi S, et al. (2011) Toll-like receptor 4 mediates alcohol-induced steatohepatitis through bone marrow-derived and endogenous liver cells in mice. *Alcohol Clin Exp Res* 35(8):1509–1518.
27. Lin SL, Kisseleva T, Brenner DA, Duffield JS (2008) Pericytes and perivascular fibroblasts are the primary source of collagen-producing cells in obstructive fibrosis of the kidney. *Am J Pathol* 173(6):1617–1627.
28. Meng F, et al. (2012) Interleukin-17 signaling in inflammatory, Kupffer cells, and hepatic stellate cells exacerbates liver fibrosis in mice. *Gastroenterology* 143(3): 765–776, e761-763.
29. Meurer SK, et al. (2013) Overexpression of endoglin modulates TGF-β1-signalling pathways in a novel immortalized mouse hepatic stellate cell line. *PLoS ONE* 8(2): e56116.
30. Parsons CJ, et al. (2011) Mutation of the 5′-untranslated region stem-loop structure inhibits α1(I) collagen expression in vivo. *J Biol Chem* 286(10):8609–8619.
31. Stefanovic B, Brenner DA (2003) 5′ stem-loop of collagen alpha 1(I) mRNA inhibits translation in vitro but is required for triple helical collagen synthesis in vivo. *J Biol Chem* 278(2):927–933.
32. Stefanovic B, et al. (1997) Posttranscriptional regulation of collagen alpha1(I) mRNA in hepatic stellate cells. *Mol Cell Biol* 17(9):5201–5209.
33. Stefanovic B, Lindquist J, Brenner DA (2000) The 5′ stem-loop regulates expression of collagen alpha1(I) mRNA in mouse fibroblasts cultured in a three-dimensional matrix. *Nucleic Acids Res* 28(2):641–647.
34. Stefanovic B, Schnabl B, Brenner DA (2002) Inhibition of collagen alpha 1(I) expression by the 5′ stem-loop as a molecular decoy. *J Biol Chem* 277(20):18229–18237.
35. Stefanovic L, Brenner DA, Stefanovic B (2005) Direct hepatotoxic effect of KC chemokine in the liver without infiltration of neutrophils. *Exp Biol Med (Maywood)* 230(8):573–586.
36. Taura K, et al. (2008) Hepatic stellate cells secrete angiopoietin 1 that induces angiogenesis in liver fibrosis. *Gastroenterology* 135(5):1729–1738.
37. Magness ST, Bataller R, Yang L, Brenner DA (2004) A dual reporter gene transgenic mouse demonstrates heterogeneity in hepatic fibrogenic cell populations. *Hepatology* 40(5):1151–1159.
38. Magness ST, Brenner DA (1999) Targeted disruption of the mouse ferrochelatase gene producing an exon 10 deletion. *Biochim Biophys Acta* 1453(1):161–174.
39. Bataller R, et al. (2003) NADPH oxidase signal transduces angiotensin II in hepatic stellate cells and is critical in hepatic fibrosis. *J Clin Invest* 112(9):1383–1394.
40. Kisseleva T, et al. (2012) Myofibroblasts revert to an inactive phenotype during regression of liver fibrosis. *Proc Natl Acad Sci USA* 109(24):9448–9453.
41. Seki E, et al. (2007) TLR4 enhances TGF-beta signaling and hepatic fibrosis. *Nat Med* 13(11):1324–1332.
42. Perepelyuk M, et al. (2013) Hepatic stellate cells and portal fibroblasts are the major cellular sources of collagens and lysyl oxidases in normal liver and early after injury. *Am J Physiol Gastrointest Liver Physiol* 304(6):G605–G614.
43. Fort MM, et al. (2001) IL-25 induces IL-4, IL-5, and IL-13 and Th2-associated pathologies in vivo. *Immunity* 15(6):985–995.
44. Gregory LG, et al. (2012) *25* drives remodelling in allergic airways disease induced by house dust mite. *Thorax* 68(1):82–90.
45. Liu Y, et al. (2011) IL-13 induces connective tissue growth factor in rat hepatic stellate cells via TGF-β-independent Smad signaling. *J Immunol* 187(5):2814–2823.
46. Pope SM, et al. (2005) Identification of a cooperative mechanism involving interleukin-13 and eotaxin-2 in experimental allergic lung inflammation. *J Biol Chem* 280(14):13952–13961.
47. Jinnin M, et al. (2006) Upregulation of tenascin-C expression by IL-13 in human dermal fibroblasts via the phosphoinositide 3-kinase/Akt and the protein kinase C signaling pathways. *J Invest Dermatol* 126(3):551–560.
48. Onitsuka I, Tanaka M, Miyajima A (2010) Characterization and functional analyses of hepatic mesothelial cells in mouse liver development. *Gastroenterology* 138(4): 1525–1535, e1521–1526.
49. Bochmann L, et al. (2010) Revealing new mouse epicardial cell markers through transcriptomics. *PLoS ONE* 5(6):e11429.
50. Asahina K (2012) Hepatic stellate cell progenitor cells. *J Gastroenterol Hepatol* 27 (Suppl 2):80–84.
51. Asahina K, et al. (2009) Mesenchymal origin of hepatic stellate cells, submesothelial cells, and perivascular mesenchymal cells during mouse liver development. *Hepatology* 49(3):998–1011.
52. Glaser SS, et al. (2007) Knockout of alpha-calcitonin gene-related peptide reduces cholangiocyte proliferation in bile duct ligated mice. *Lab Invest* 87(9):914–926.
53. Chang K, Pastan I (1996) Molecular cloning of mesothelin, a differentiation antigen present on mesothelium, mesotheliomas, and ovarian cancers. *Proc Natl Acad Sci USA* 93(1):136–140.
54. Grigoriu BD, Grigoriu C, Chahine B, Gey T, Scherpereel A (2009) Clinical utility of diagnostic markers for malignant pleural mesothelioma. *Monaldi Arch Chest Dis* 71(1): 31–38.
55. Bera TK, Pastan I (2000) Mesothelin is not required for normal mouse development or reproduction. *Mol Cell Biol* 20(8):2902–2906.
56. Lujambio A, et al. (2013) Non-cell-autonomous tumor suppression by p53. *Cell* 153(2): 449–460.
57. Krizhanovsky V, et al. (2008) Senescence of activated stellate cells limits liver fibrosis. *Cell* 134(4):657–667.
58. Henderson NC, et al. (2013) Targeting of αv integrin identifies a core molecular pathway that regulates fibrosis in several organs. *Nat Med* 19(12):1617–1624.
59. Mederacke I, et al. (2013) Fate tracing reveals hepatic stellate cells as dominant contributors to liver fibrosis independent of its aetiology. *Nat Commun* 4:2823.
60. Asahina K, Zhou B, Pu WT, Tsukamoto H (2011) Septum transversum-derived mesothelium gives rise to hepatic stellate cells and perivascular mesenchymal cells in developing mouse liver. *Hepatology* 53(3):983–995.
61. Desmoulière A (2007) Hepatic stellate cells: The only cells involved in liver fibrogenesis? A dogma challenged. *Gastroenterology* 132(5):2059–2062.
62. Tang L, Tanaka Y, Marumo F, Sato C (1994) Phenotypic change in portal fibroblasts in biliary fibrosis. *Liver* 14(2):76–82.
63. Tuchweber B, Desmoulière A, Bochaton-Piallat ML, Rubbia-Brandt L, Gabbiani G (1996) Proliferation and phenotypic modulation of portal fibroblasts in the early stages of cholestatic fibrosis in the rat. *Lab Invest* 74(1):265–278.
64. Syal G, Fausther M, Dranoff JA (2012) Advances in cholangiocyte immunobiology. *Am J Physiol Gastrointest Liver Physiol* 303(10):G1077–G1086.
65. Fickert P, et al. (2009) Farnesoid X receptor critically determines the fibrotic response in mice but is expressed to a low extent in human hepatic stellate cells and periductal myofibroblasts. *Am J Pathol* 175(6):2392–2405.
66. Fausther M, Dranoff JA (2011) New insights on the pathogenesis of biliary cirrhosis provided by studies in FXR knockout mice. *J Hepatol* 55(4):939–940.
67. Guyot C, et al. (2010) Fibrogenic cell phenotype modifications during remodelling of normal and pathological human liver in cultured slices. *Liver Int* 30(10):1529–1540.
68. Keitel V, et al. (2009) The membrane-bound bile acid receptor TGR5 is localized in the epithelium of human gallbladders. *Hepatology* 50(3):861–870.
69. Fabris L, Strazzabosco M (2011) Epithelial-mesenchymal interactions in biliary diseases. *Semin Liver Dis* 31(1):11–32.
70. Wynn TA (2003) IL-13 effector functions. *Annu Rev Immunol* 21:425–456.
71. Liu Y, Munker S, Müllenbach R, Weng HL (2012) IL-13 signaling in liver fibrogenesis. *Front Immunol* 3:116.
72. Roderfeld M, et al. (2012) Bone marrow transplantation improves hepatic fibrosis in Abcb4-/- mice via Th1 response and matrix metalloproteinase activity. *Gut* 61(6): 907–916.
73. Enzan H, et al. (1997) Development of hepatic sinusoidal structure with special reference to the Ito cells. *Microsc Res Tech* 39(4):336–349.
74. Zhou B, et al. (2008) Epicardial progenitors contribute to the cardiomyocyte lineage in the developing heart. *Nature* 454(7200):109–113.
75. Hassan R, Bera T, Pastan I (2004) Mesothelin: A new target for immunotherapy. *Clin Cancer Res* 10(12 Pt 1):3937–3942.
76. Scholler N, et al. (1999) Soluble member(s) of the mesothelin/megakaryocyte potentiating factor family are detectable in sera from patients with ovarian carcinoma. *Proc Natl Acad Sci USA* 96(20):11531–11536.
77. Sapede C, et al. (2008) Aberrant splicing and protease involvement in mesothelin release from epithelioid mesothelioma cells. *Cancer Sci* 99(3):590–594.
78. Woo K, et al. (2010) Adenosine triphosphate release and purinergic (P2) receptor-mediated secretion in small and large mouse cholangiocytes. *Hepatology* 52(5): 1819–1828.

Supporting Information

Iwaisako et al. 10.1073/pnas.1400062111

SI Materials and Methods

Immunocytochemistry. Isolated cells were fixed in 4% (wt/vol) paraformaldehyde in PBS and stained anti-desmin Ab (Thermo Scientific), anti-glial fibrillar acidic protein (GFAP) (Dako), and anti-synemin (gift of A. Geerts, Laboratory for Cell Biology, Vrije Universiteit Brussel, Brussel-Jette, Belgium). Anti-mouse Endoglin (CD105) Ab, anti-CD45, anti-MHC II Ab, anti-F4/80 Ab, anti-CD11b Ab, anti-CD146, anti-Thy1 Ab (eBioscience), TE-7 Ab (anti-elastin Ab; Millipore), or isotype control was followed by secondary Alexa Fluor 594 antibodies and nuclei costaining with DAPI. Collagen GFP expression was visualized by fluorescent microscopy. Immunocytostaining with TE-7 Ab was performed by using MOM kit (Vector).

Whole Mouse Genome Gene Expression Microarray. The gene expression profile of bile duct ligation (BDL)- (20 d) activated hepatic stellate cells (aHSCs) and activated portal fibroblasts (aPFs) was compared with carbon tetrachloride- (CCl_4) aHSCs was studied by using Whole Mouse Genome Microarray (Agilent). mRNA was purified by using RNAeasy columns (Qiagen), 160 ng of purified RNA per sample was labeled by using the LRILAK PLUS, two color low RNA input Linear Amplification kit, and hybridized to a Whole Mouse Genome Microarray 4×44K 60-mer slide according to the manufacturer's instructions (Agilent). Slides were scanned by using the Agilent GZ505B Scanner and analyzed by using the Gene Spring Software (Agilent). Hierarchical clustering of gene expression values was performed by using Cluster 3.0 (http://bonsai.hgc.jp/~mdehoon/software/cluster/software.htm; ref. 1) using the correlation coefficient as the similarity metric, and average linkage when merging nodes during tree building. Clustering was performed on genes expressed in at least one condition (>9 $\log_2$ intensity value) to remove absent genes and genes exhibiting a SD greater than 0.75 among $\log_2$ intensity values to remove genes with constant expression. Hierarchical clustering results were visualized by using Java Tree View (2). Differentially regulated genes were defined as those with significant absolute expression (>9 $\log_2$ intensity value) and exhibiting twofold compared with the maximal value in all other samples. Gene ontology and KEGG pathway functional enrichment analysis was performed by using DAVID (http://david.abcc.ncifcrf.gov; ref. 3).

1. de Hoon MJ, Imoto S, Nolan J, Miyano S (2004) Open source clustering software. *Bioinformatics* 20(9):1453–1454.
2. Saldanha AJ (2004) Java Treeview—extensible visualization of microarray data. *Bioinformatics* 20(17):3246–3248.
3. Dennis G, Jr, et al. (2003) DAVID: Database for Annotation, Visualization, and Integrated Discovery. *Genome Biol* 4(5):3.

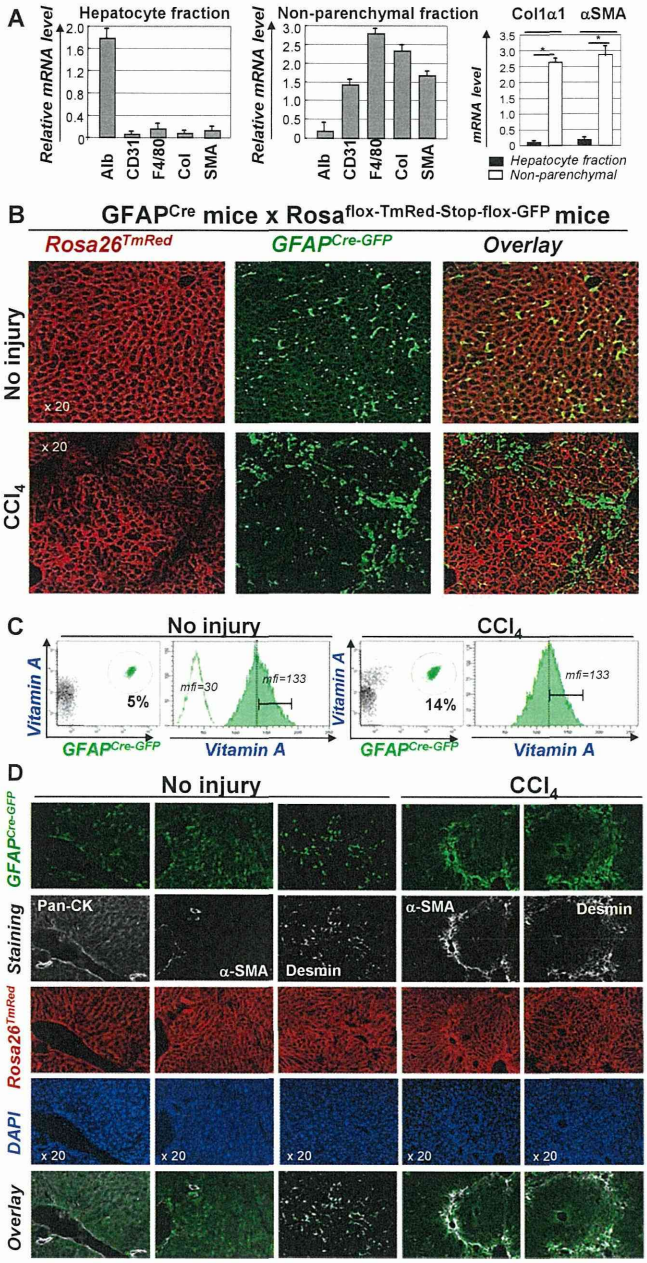

Fig. S1. Hepatic myofibroblasts are isolated in nonparenchymal fraction from BDL Col-GFP mice. (*A*) Analysis of nonparenchymal fraction from BDL-injured Col-GFP mice by RT-PCR. The total myofibroblast population from BDL- and CCl_4-injured Col-GFP mice was isolated in the fraction of nonparenchymal liver cells. Nonparenchymal fraction (but not hepatocyte fraction) contained Cola1a$^+$ and α-SMA$^+$ cells. Nonparenchymal fraction contained myeloid cells (F4/80), endothelial cells (CD31), and myofibroblasts (Col and α-SMA). The data shows relative mRNA level, normalized for 18S, $P < 0.01$. (*B*) GFAP$^{Cre\text{-}GFP}$ mice were generated by crossing GFAP^{Cre} mice with Rosa26$^{flox\text{-}mTRed\text{-}Stop\text{-}flox\text{-}mGFP}$ mice. Livers from GFAP$^{Cre\text{-}GFP}$ mice (no injury, $n = 5$; CCl_4-treated, $n = 5$) were analyzed by fluorescent microscopy, and genetically labeled HSCs were visualized as membrane tagged GFP$^+$ (mTRed$^-$) cells. Cells that did not express GFAP-driven Cre were visualized by TmRed color. (*C*) Nonparenchymal fraction from uninjured and CCl_4-injured GFAP^{Cre} x Rosa26$^{flox\text{-}mTRed\text{-}Stop\text{-}flox\text{-}mGFP}$ mice were analyzed by flow cytometry for the presence of vitamin A in quiescent and activated HSCs. GFAP-expressing HSCs were visualized by GFP expression (488 nm), and Vit.A$^+$ cells were visualized by autofluorescent signal (405 nm) detected by violet laser. Although expression of Vinamin A was down-regulated in aHSCs (compared with qHSCs), vitamin A was still detected in aHSCs. Representative dot plots and histograms are shown ($n = 5$ mice per group). (*D*) Cell fate mapping of GFAP^{GFP+} qHSCs and aHSCs. In agreement with most previous reports (1–3), but in contrast to others (4, 5), we did not observe any leakiness of GFAP-driven Cre expression into epithelial cells. No GFAP$^+$ cells expressed Pan-cytokeratin (Pan-CK) marker of cholangiocytes, but GFAP$^+$ cells coexpressed desmin. As expected, these GFAP$^+$ HSCs up-regulated expression of α-SMA in response to CCl_4. Expression of GFP overlapped (>90%) with α-SMA and desmin staining. In concordance with other reports (2, 6), GFAP-Cre is suitable for genetic labeling of HSCs.

1. Meng F, et al. (2012) Interleukin-17 signaling in inflammatory, Kupffer cells, and hepatic stellate cells exacerbates liver fibrosis in mice. *Gastroenterology* 143(3):765–776 e761-763.
2. Scholten D, et al. (2011) Migration of fibrocytes in fibrogenic liver injury. *Am J Pathol* 179(1):189–198.
3. Bataller R, Brenner DA (2005) Liver fibrosis. *J Clin Invest* 115(2):209–218.
4. Yang L, et al. (2008) Fate-mapping evidence that hepatic stellate cells are epithelial progenitors in adult mouse livers. *Stem Cells* 26(8):2104–2113.
5. Mederacke I, et al. (2013) Fate tracing reveals hepatic stellate cells as dominant contributors to liver fibrosis independent of its aetiology. *Nat Commun* 4:2823.
6. Hernández-Gea V, et al. (2012) Autophagy releases lipid that promotes fibrogenesis by activated hepatic stellate cells in mice and in human tissues. *Gastroenterology* 142(4):938–946.

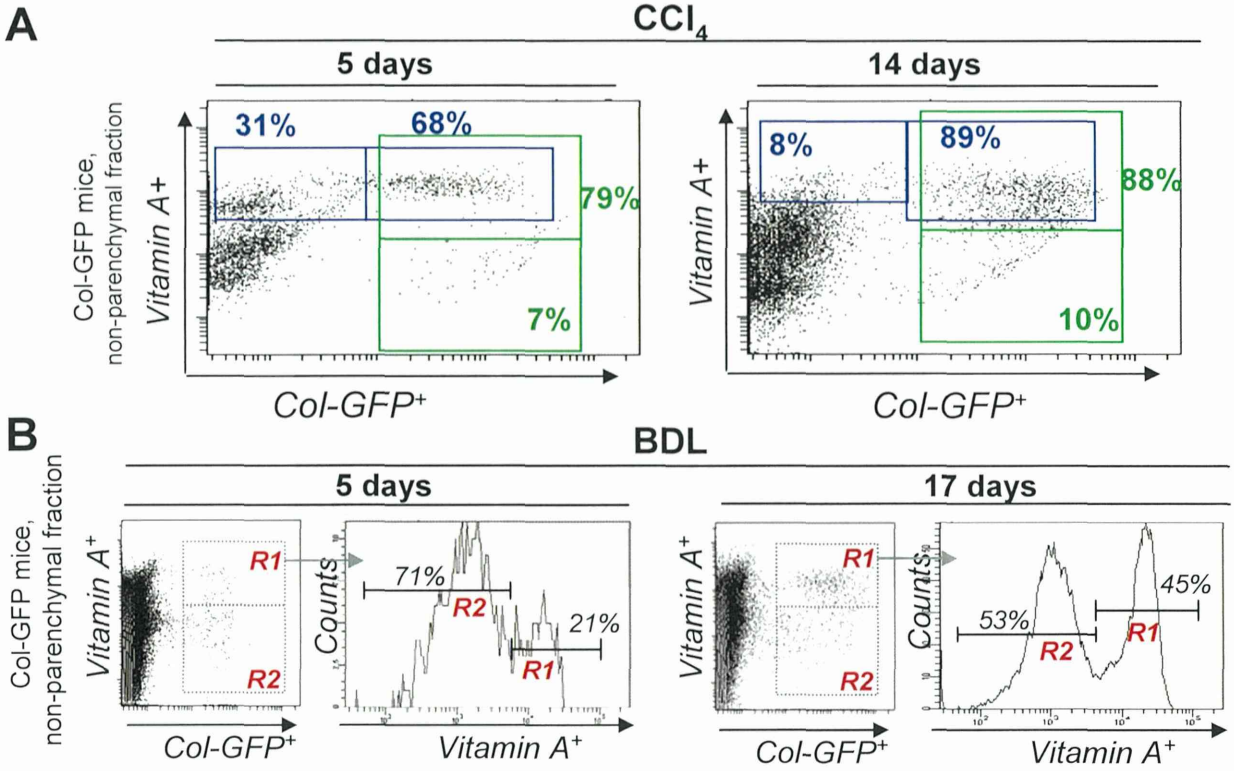

Fig. S2. Analysis of GFP$^+$ myofibroblasts at early time points of CCl_4 and BDL injury. (*A*) aHSCs are the major source of myofibroblasts in response to CCl_4-induced liver injury. Nonparenchymal fraction was isolated from Col-GFP mice after 5 d and 2 wk of CCl_4 and analyzed by flow cytometry for the presence of GFP$^+$Vit.A$^+$ and GFP$^+$Vit.A$^+$ myofibroblasts. (*B*) Nonparenchymal fraction from Col-GFP mice were analyzed after 5 d and 17 d of BDL. Representative dot plots are shown. GFP$^+$ myofibroblasts were further analyzed for the presence of Vit.A$^+$ (gate R1) and Vit.A$^-$ (gate R2) cells by histograms, $P < 0.01$.

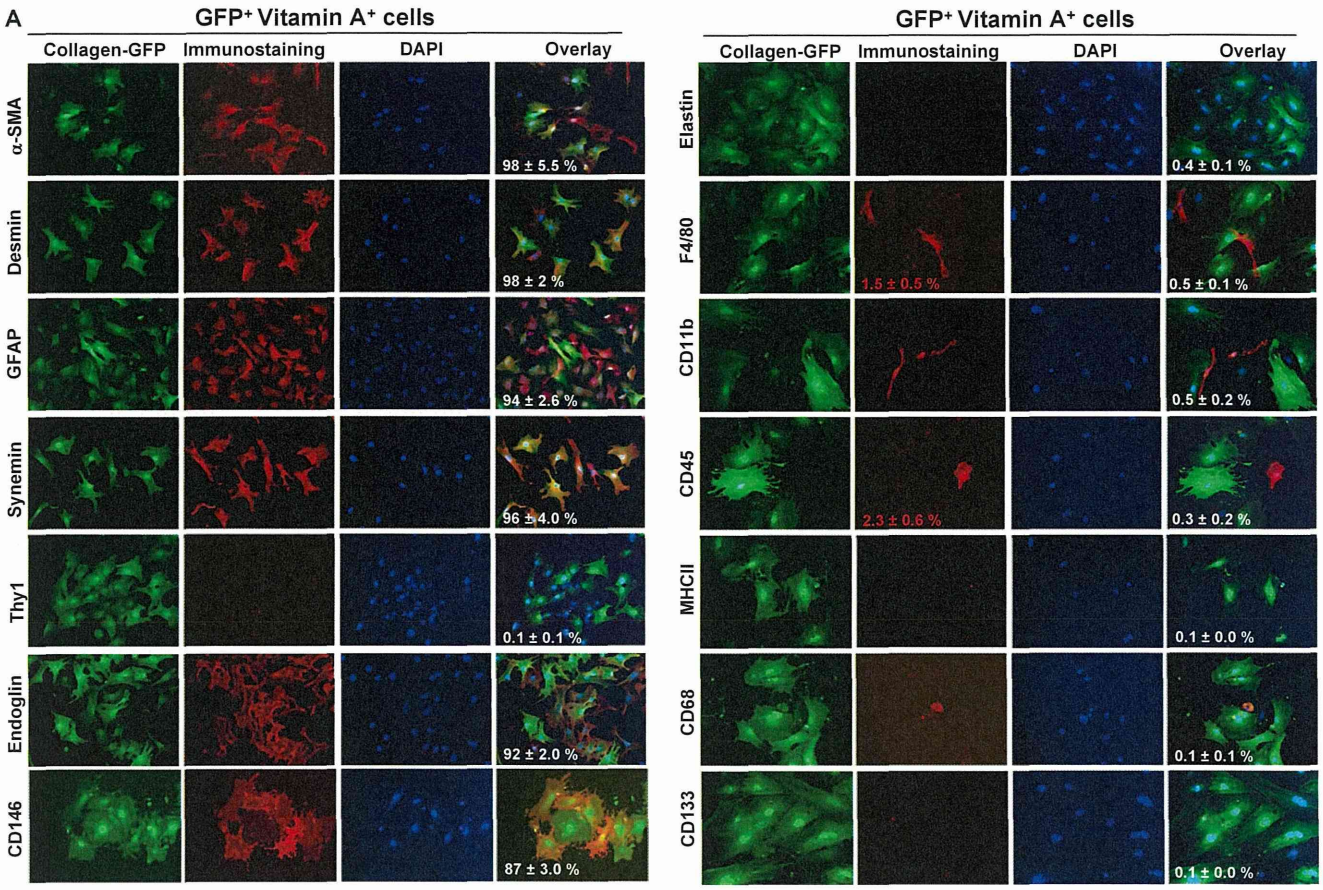

Fig. S3. (Continued)

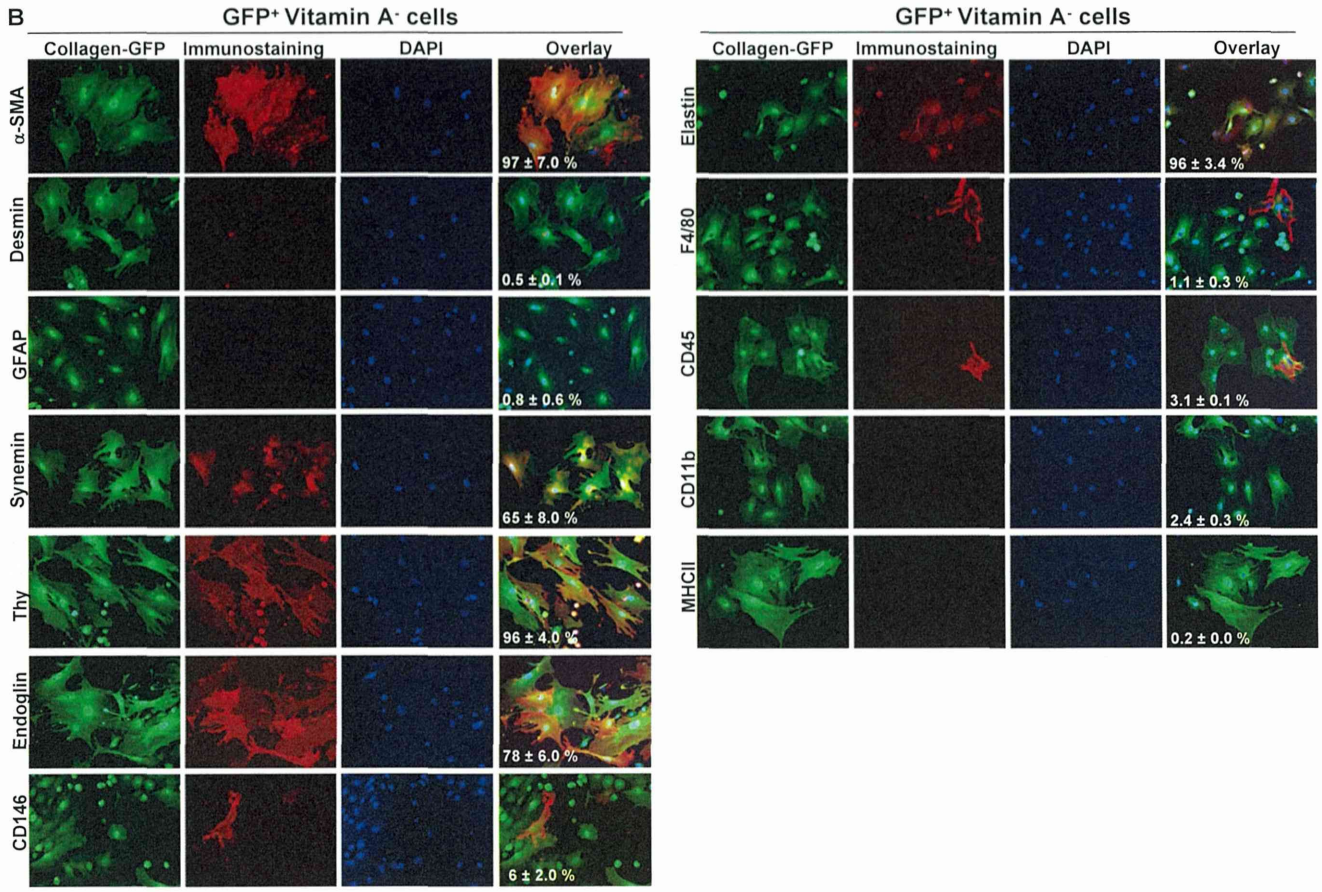

Fig. S3. Immunophenotyping of GFP$^+$ myofibroblasts isolated from CCl_4-treated mice. (*A*) GFP$^+$Vit.A$^+$ cells were sort purified from nonparenchymal fractions of CCl_4- (1.5 mo) treated Col-GFP mice and immunophenotyped. Expression of myofibroblast marker (α-SMA), HSC markers (desmin, GFAP, CD146, synemin), PF markers (elastin, Thy1), hematopoietic markers (CD45, F4/80, CD68, CD11b), and endoglin was analyzed by immunofluorescence using specific antibodies or isotype matched control (data not shown). GFP labels collagen-expressing cells and DAPI stains nuclei (40× objective). GFP$^+$Vit.A$^+$ were identified as aHSCs, and the percent of positively stained cells is calculated (compared with total cells, 100%, $P < 0.05$). (*B*) Similar immunophenotyping was performed for GFP$^+$Vit.A$^-$ cells isolated by cell sorting from nonparenchymal fractions of CCl_4- (1.5 mo) treated Col-GFP mice. GFP$^+$Vit.A$^-$ cells were identified as aPFs, and the percent of positively stained cells is calculated (compared with total cells, 100%, $P < 0.01$). Of technical interest, both GFP$^+$Vit.A$^+$ and GFP$^+$Vit.A$^-$ myofibroblasts were stained positive for synemin and endoglin (CD105), suggesting that these markers do not discriminate between aHSCs and aPFs.

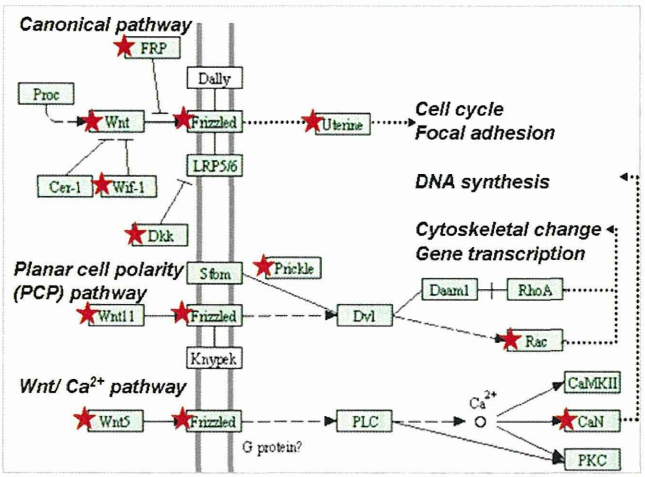

Fig. S4. Wnt signaling pathway is induced in BDL-aPFs. The following signaling pathways were up-regulated in aPFs using GO TERM analysis of aPFs (BDL, 20 d) subjected to the whole mouse genome microarray: ECM-interaction (16 genes, $P < 7.1e^{-5}$), focal adhesion (16 genes, $P < 5.2e^{-3}$), cell adhesion molecules (18 genes, $P < 7.2e^{-3}$), pathways in cancer (30 genes, $P < 1.2e^{-2}$), regulation of actin cytoskeleton (22 genes, $P < 1.4e^{-2}$), Wnt signaling (15 genes, $P < 5.1e^{-2}$), and renin-angiotensin system (7 genes, $P < 8.0e^{-5}$) signaling pathways. Activation of Wnt signaling pathway is shown, and Wnt signaling genes that are induced in aPFs are marked with red stars.

SIGNATURE GENES :			
Maximum ↑ HSCs (BDL)	**Fold**	**Maximum ↑ HSCs (CCl_4)**	**Fold**
Succinate receptor 1 (Sucnr1)	3.6	28S ribosomal RNA LOC236598	15
Chloride channel Clca1 and 2	3 & 2.8	Hexokinase 2 (Hk2)	10
Nexin 1 (Nrxn1)	2.9	Trombospodin 1 (Thbs1)	16
Integrin 2β (Itga2b)	3.0	α-smooth muscle actin Acta2 and Acta1	3 & 6
Hedgehod-interacting protein (Hhip)	3.0	Nestin	7.4
Netrin 1 (Ntn1)	0.35	Cytochrome P450 (Cyp17a1	4.7
Complement factor D (adipsin, Cfd)	4.3	Transgelin (Tagln)	2.0
Angiotensin II receptor (Agtr1a)	2.3	Nuclear factor IL-3 regulated (Nfil3)	4.3
Snail homolog 2 (Snai2)	2.4	Lactalbumin (Lalba)	6.2
Neurotrophin 3 (Ntf3)	2.0	Lectin (Lgals)	2.4
Synaptptotagmin IX (Syt9)	1.4	Tubulin β6 (Tubb6)	2.8
T-box 20 (Tbx20)	1.3	γ2-smooth muscle actin (Actg2)	2.6
FGF-R2	1.4	Metalloprotein 1 (Mt1)	1.6
Dispatched Homolog 2 (Disp2)	1.5	Tubulin β5 (Tubb5)	2.3
Desert Hedgehog (Dhh)	1.6	Syndecan 4 (Sdc4)	2.9
TGF-α	1.5	MMP-10	5.8
NGF-R and NGF	1 & 1.8	Cyclin L1 (Ccnl1)	4.5
Tribbles Homolog 2 (Trib2)	1.3	Col1a2	1.2
Talin 2 (Tln2)	0.7	Leucyl-tRNA synthetase (Lars2)	1.4
CD38	1.8	Cdkn1a	2.7
Sprouty Homolog 1 (Spry1)	2.7	Filamin α (Flna)	1.6
Roundabout homolog 2	0.34	Cox7b	2.1
Glipican 4	1.2	Kruppel-like factor2 (Klf2)	2.0
Iron transporter Slc40a1	2.0	Fibrillarin (Fbl)	2.0
CD40	1.1	Myocyte enhancer factor Mef2c	3.0
Notch 4	1.7	Col1al	1.3
CD36	1.8	Tubulin α1A (Tuba1a)	1.4
PDGF-Rβ	1.2	Calreticulin (Calr)	1.4
Smad5	1.9	Laminin (Lmna)	1.8

Fig. S5. Differential expression of genes up-regulated in BDL-aHSCs and CCl_4-aHSCs. Using the whole mouse genome microarray, expression of genes differentially expressed in BDL (20 d)- aHSCs and CCl_4-aHSCs was determined. Fold induction is calculated compared with the highest value observed in BDL-aPFs and BDL-aHSCs (or CCl_4-activated HSCs). In addition, we determined that CCl_4-aHSCs exhibited a more activated phenotype, as determined by stronger up-regulation of fibrogenic genes Acta 1 (fold induction >4), Acta 2 (>6), Cola1 (>2.1), and Cola2 (>2.7) and in replication associated genes ribosomal RNA LOC236598 (>15 28S), cyclin L1 (>2.7), and Cdkn1a (>2.6) (over the mRNA levels detected in BDL-induced aHSCs or aPFs). In turn, BDL-aHSCs highly expressed neural markers (>7.6 nexin, >5.4 netrin, >4.7 neurotrophin 3, >7.2 synaptotagmin IX), Hedgehog family of genes (>5.8 Hhip, >4.8 Snai2, >3.8 Disp2, >3.2 Dhh, >3.2 Trib2, >2.5 Spry1), CD40, and FGF-R2, which distinguished them from CCl_4-aHSCs and BDL-aPFs. Thus, CCl_4 induces stronger activation of HSCs in vivo than BDL.